Laser Chem. Vol. 10, pp. 109–138
Reprints available directly from the Publisher
Photocopying permitted by license only

EFFECTS OF MOLECULAR VIBRATION AND ROTATION ON INTRAMOLECULAR DYNAMICS IN S_1 OF *s*-TRIAZINE VAPOR

NOBUHIRO OHTA

Division of Chemistry, Research Institute of Applied Electricity, Hokkaido University, Sapporo 060, Japan

(Received 15 September, 1988; in final form 14 November, 1988)

Emission properties of *s*-triazine vapor have been examined for excitation into various vibronic levels of S_1. The emission involves broad fluorescence besides the sharp fluorescence emitted from the initially prepared vibronic level (IPL). At low pressures, the IPL fluorescence exhibits a biexponential decay composed of fast and slowly decaying portions, and the broad fluorescence also consists of fast and slow components with lifetimes comparable to those of the IPL fluorescence. The broad fluorescence exhibits another slow component, which is characterized by a less tendency to undergo collisional quenching. The emitting levels of the broad fluorescence are regarded as reached directly from the IPL and indirectly via triplet state. The quantum yield of the slow component of the IPL fluorescence remarkably depends on the rotational level excited, whereas the quantum yield of the broad fluorescence is nearly independent of the rotational level excited. These results suggest that K scrambling occurs not only in the intersystem crossing between singlet and triplet levels but also in the relaxation to other singlet levels from the IPL.

KEY WORDS: s-triazine, IPL, fluorescence, K Scrambling.

1. INTRODUCTION

Yields and decays of fluorescence emitted from the initially prepared vibronic level (IPL) of 6^1 or 6^2 in S_1 of *s*-triazine vapor were carefully examined both in the bulk gas and in a supersonic jet.[1,2] The fluorescence quantum yields at low pressures were shown to exhibit a remarkable variation along the rotational contour with a sharp peak near the band origin.[1] The lifetimes of the slow component of fluorescence were also shown to vary remarkably along the rotational contour with a minimum near the origin.[1,2] The observed rotational level dependence of the yields and decays of the fluorescence was attributed to a difference of the number of the triplet levels coupled to the singlet ro-vibronic level excited,[1,2] based on the singlet-triplet mixed state model.[3,4]

As reported preliminary in previous papers,[5,6] however, *s*-triazine vapor exhibits a broad emission besides the fluorescence emitted from the IPL. The broad emission is considered to be emitted from singlet levels other than the IPL. For through understanding of the intramolecular dynamics of *s*-triazine vapor following excitation into S_1, therefore, it will be necessary to examine the properties not only of the

fluorescence emitted from the IPL but also of the broad emission for excitation into the individual rotation-vibration levels.

In the present study, yields and decays of the broad emission besides the fluorescence from the IPL have been examined at various pressures on excitation into the individual vibronic levels belonging to S_1 which lie below 62,000 cm^{-1} above the S_1 origin. In addition to the excited level dependence of the fluorescence quantum yield, excited level dependence of the triplet formation yield has been also examined, based on the measurements of the sensitized biacetyl phosphorescence quantum yield. On the basis of these results, effects of molecular vibration and rotation on intramolecular dynamics following excitation into S_1 of *s*-triazine vapor are discussed.

2. EXPERIMENTAL

s-Triazine and biacetyl (Nakarai Chemicals) were purified by vacuum sublimation and vacuum distillation, respectively. Commercially available sulfur hexafluoride (SF_6) was used without further purification as an inert foreign gas. The pressure of *s*-triazine was determined by using a capacitance manometer (MKS Baratron type 170) or by measuring the absorption intensity.

All the optical measurements were carried out at room temperature. Absorption and emission–excitation spectra at low spectral resolution were measured with a Cary 15 spectrophotometer and an emission spectrophotometer,[7] respectively. Absorption and emission–excitation spectra at high spectral resolution, emission spectra and emission decays were measured with a laser spectrophotometric system.[8] The procedures for the latter measurements are essentially the same as those reported in previous papers,[1,9] and the emission dispersed by a monochromator (Nikon G-250) was monitored. The frequency of a pulsed dye laser (Molectron DL14) pumped by a nitrogen laser (UV22) was doubled by a KDP crystal. The generated UV pulses, which were used for exciting the sample, have a linewidth of ~0.5 cm^{-1} and a duration of ~3 ns. Emission measurements were made with a 3.5 cm cubic quartz cell, and absorption spectra were measured by the use of a cylindrical cell with a diameter of 3 cm and a length of 10 cm or 30 cm.

The excitation spectra were corrected for the spectral intensity distribution of the exciting light and for the inner filter effect by using a solution of rhodamine B. The absolute quantum yield was determined by comparing the emission spectrum of *s*-triazine vapor with that of quinine bisulfate in a 1 *N* sulfuric acid.[10] The correction of the emission spectrum for the spectral sensitivity of the detection system was made by using a solution of quinine bisulfate and β-naphthol.[11]

Fluorescence decays were measured with a single-photon counting lifetime apparatus equipped with a time-to-amplitude converter, by using the laser system mentioned above.[8] Excitation position is the peak of the rotational contour of the individual vibronic absorption bands, unless otherwise noted. For the measurements of the emission decays of the fast component, a picosecond laser system was used as an excitation light source, which is composed of a synchronously pumped, cavity-

dumped dye laser (Spectra Physics 375 and 344S) and a mode-locked argon-ion laser (Spectra Physics 171–18).[12] Frequency-doubled UV pulses with a linewidth of 5 cm^{-1} and a duration of 6 ps (fwhm) were generated through a KDP crystal with a repetition rate of 800 kHz.

3. RESULTS

3.1 *Absorption and Fluorescence Spectra*

Absorption spectrum of *s*-triazine vapor in the region from 320 nm to 230 nm is shown in Figure 1. The sharp bands observed in the longer-wavelength region were assigned to the $S_0 \rightarrow S_1$ vibronic bands.[13–15] Note that S_1 was assigned to the $^1E''(n\,\pi^*)$ state.[13–15] Figure 2 shows the rotational contour of the individual vibronic absorption bands. As is immediately known in Figure 2, lower vibronic bands exhibit a parallel-type rotational contour characterized by a strong *Q*-branch.[14] Higher vibronic bands are also known to exhibit a parallel-type rotational contour, but the contour becomes complex and broader with shortening the excitation wavelength. The increase of the absorption bandwidth suggests that the rate of some intramolecular dynamics which occurs from the IPL becomes faster with increasing the excess vibrational energy above the S_1 origin (ΔE).

Figure 3 shows emission spectra of *s*-triazine vapor on excitation at the *Q*-branch peak of representative vibronic bands belonging to the $S_0 \rightarrow S_1$ transition. For excitation into lower vibronic levels of 6^1 and 6^2, emission spectra with a sharp

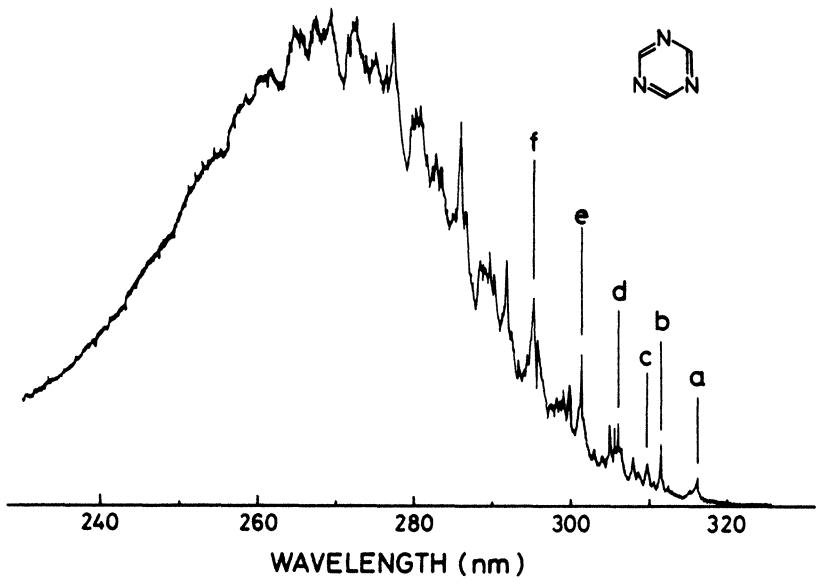

Figure 1 Absorption spectrum of *s*-triazine vapor at room temperature obtained with a spectral resolution of 0.1 nm.

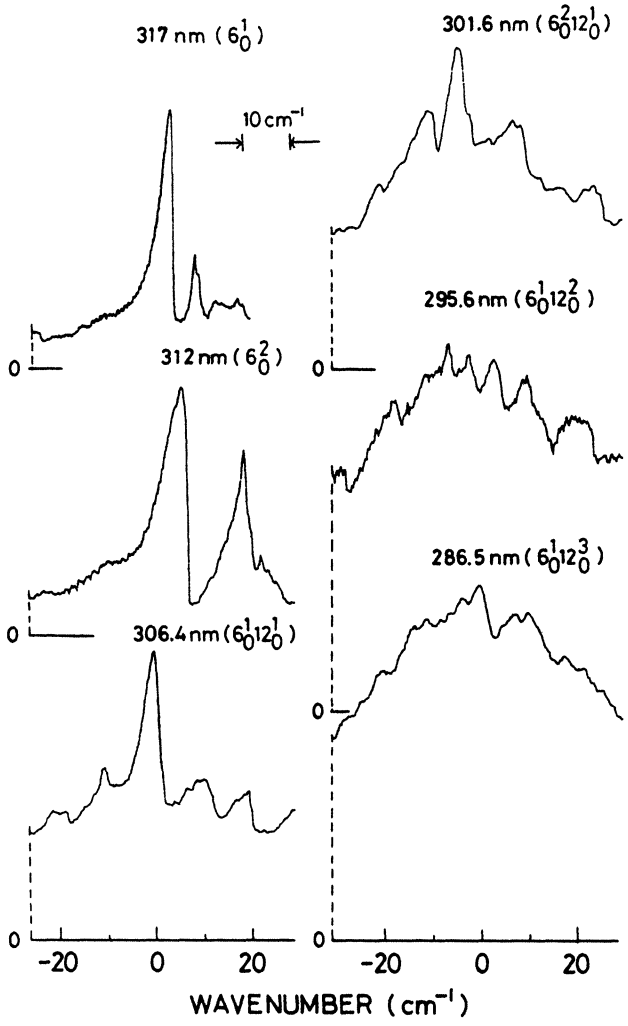

Figure 2 Rotational contour of the individual vibronic absorption bands belonging to the $S_0 \rightarrow S_1$ transition of 2s-triazine vapor obtained with a spectral resolution of ~0.5 cm^{-1}. In each spectrum, the base line is indicated by 0.

structure are observed. As ΔE increases, however, the intensity of a broad emission with a maximum at around 400 nm relative to the intensity of the sharp emission bands abruptly increases, and no sharp band appears on excitation at wavelengths below 300 nm. As mentioned previously, the sharp emission can be assigned to the fluorescence emitted from the IPL and the broad emission is considered to originate from the vibronic level(s), denoted by U, to which a non-radiative transition occurs from the IPL. Hereafter, these emissions are called as IPL fluorescence and broad fluorescence, respectively, and the nonradiative transition from the IPL to U is called

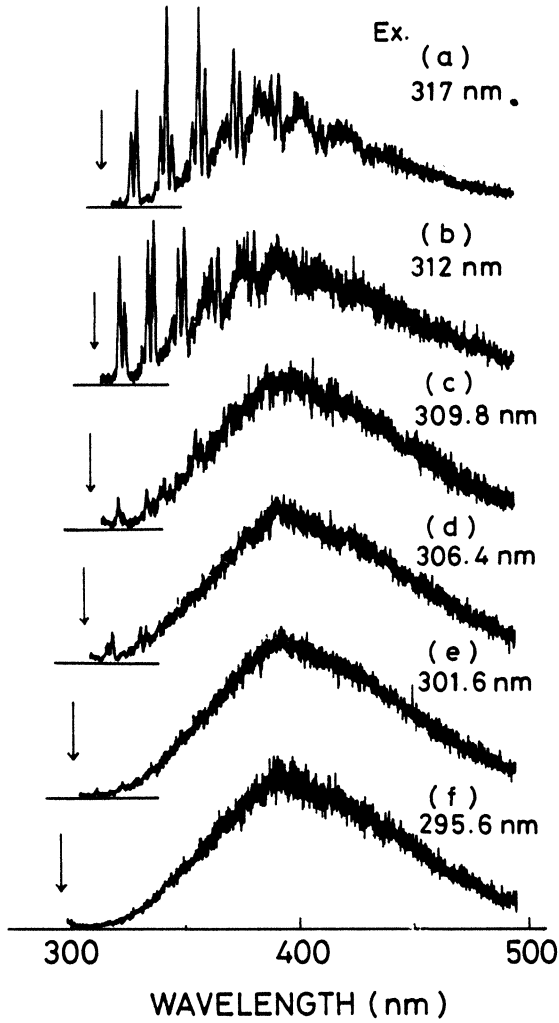

Figure 3 Emission spectra of *s*-triazine vapor at 4.5 Torr on excitation at various $S_0 \rightarrow S_1$ vibronic bands. These spectra are uncorrected for the spectral sensitivity of the detection system. Excitation positions (*a*)–(*f*), which correspond respectively to the peaks *a*–*f* in Figure 1, are shown by arrows.

as IVR. The abrupt increase of the intensity of the broad fluorescence relative to the IPL fluorescence suggests that IVR rate abruptly increases with increase of ΔE. The fluorescence polarization measurements indicates that the broad fluorescence appears even for excitation into the lower vibronic level of 6^1, as reported in a previous paper.[16]

Pressure dependence of the emission spectra has been examined. As the pressure increases, the intensity of the broad fluorescence relative to the IPL fluorescence slightly increases for any excitation.

3.2. *Fluorescence Excitation Spectra and Fluorescence Quantum Yields*

Emission excitation spectra of *s*-triazine vapor in the $S_0 \rightarrow S_1$ absorption region were obtained at various pressures with an excitation bandwidth of 0.3 nm. These spectra are shown in Figure 4. The corresponding absorption spectrum in the same region is also shown in Figure 4. At low pressures below one Torr, the emission of

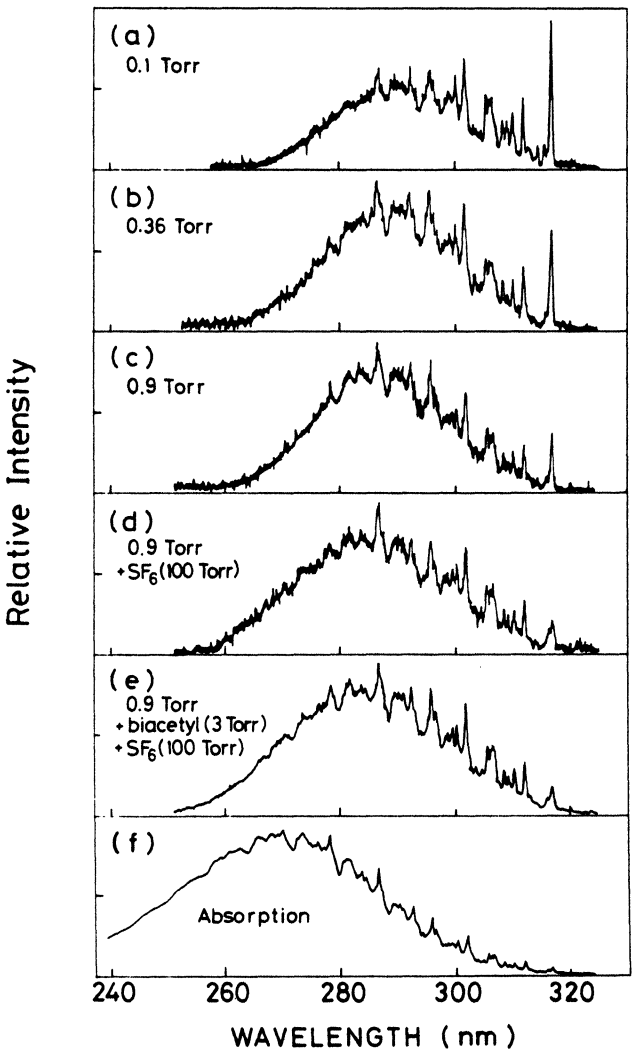

Figure 4 Emission excitation spectra of *s*-triazine vapor at various pressures: (*a*) 0.1 Torr; (*b*) 0.36 Torr; (*c*) 0.9 Torr; (*d*) 0.9 Torr in the presence of 100 Torr of SF_6; (*e*) 0.9 Torr in the presence of 3 Torr of biacetyl and 100 Torr of SF_6. The spectra in (*a*)–(*d*) and in (*e*) were obtained by monitoring the total emission and the sensitized biacetyl phosphorescence, respectively. These spectra are uncorrected for the spectral intensity distribution of the exciting light. The corresponding absorption spectrum is also shown in (*f*).

s-triazine is dominated by the fluorescence, and the spectra shown in Figures 4(*a*)–(*c*), which were obtained by monitoring the total emission at 0.1, 0.36 and 0.9 Torr respectively, correspond to the fluorescence excitation spectra. As the pressure is reduced, the shorter-wavelength bands become weak in comparison with the longer-wavelength ones, as is seen in Figure 4. At high pressures above several Torr, phosphorescence of *s*-triazine vapor with a lifetime of 7.1 μs is observed besides the fluorescence.[17] Accordingly, the spectrum shown in Figure 4(*d*), which was obtained at 0.9 Torr in the presence of 100 Torr of added SF_6, is regarded as the fluorescence excitation spectrum superimposed by the phosphorescence excitation spectrum. The intensity of the phosphorescence relative to the total emission intensity is 0.32 at 100 Torr on excitation at 286.5 nm, as is known from the emission decay shown in Figure 2 of Ref. 17. Then, the phosphorescence intensities at other excitation positions were evaluated by employing the sensitized biacetyl phosphorescence excitation spectrum shown in Figure 4(*e*) instead of the phosphorescence excitation spectrum. The phosphorescence intensity thus obtained was subtracted from the total emission intensity to evaluate the fluorescence intensity at various excitation positions. These fluorescence intensities were converted to the absolute fluorescence quantum yield with a procedure mentioned in the experimental section.

The pressure dependence of the fluorescence quantum yield in the $S_0 \rightarrow S_1$ absorption region is shown in Figure 5. As the pressure increases, the yield decreases at any excitation position, but the yield is not affected by a change in pressure above 100 Torr. The pressure dependence of the fluorescence quantum yield suggests that *s*-triazine belongs to the intermediate case molecule which exhibits fluorescence composed of fast and slowly decaying portions and that only the slow component is well quenched by a collision, as in the case of pyrazine[18] and pyrimidine.[19,20]

The fluorescence quantum yield $\Phi_F(p)$ as a function of p can then be written as

$$\Phi_F(p) = \Phi_{F_1} + \Phi_{F_2}(p) \tag{1}$$

where 1 and 2 refer to the fast and slow components, respectively. The values of $\Phi_F(p)$ at $p = 100$ Torr are regarded as equal to the Φ_{F_1} values. The values of Φ_{F_1} thus obtained are shown in *Table 1*. As mentioned above, the fluorescence emission consists of the IPL fluorescence and the broad fluorescence. Thus, Φ_{F_1} and $\Phi_{F_2}(p)$ are represented as follows:

$$\Phi_{F_1} = \Phi_{F_1}^{\mathrm{IPL}} + \Phi_{F_1}^{\mathrm{broad}} \tag{2}$$

$$\Phi_{F_2}(p) = \Phi_{F_2}^{\mathrm{IPL}}(p) + \Phi_{F_2}^{\mathrm{broad}}(p) \tag{3}$$

where IPL and broad refer to the IPL and broad fluorescence emissions, respectively. As is seen in *Table 1*, Φ_{F_1} varies on ΔE, but it may be assumed that, for a particular value of ΔE, both $\Phi_{F_1}^{\mathrm{IPL}}$ and $\Phi_{F_1}^{\mathrm{broad}}$ are approximately constant within the pressure range studied. Then, the $\Phi_{F_2}\mathrm{A}(p)$ values can be determined by subtracting the $\Phi_F(p)$ at $p = 100$ Torr from $\Phi_F(p)$.

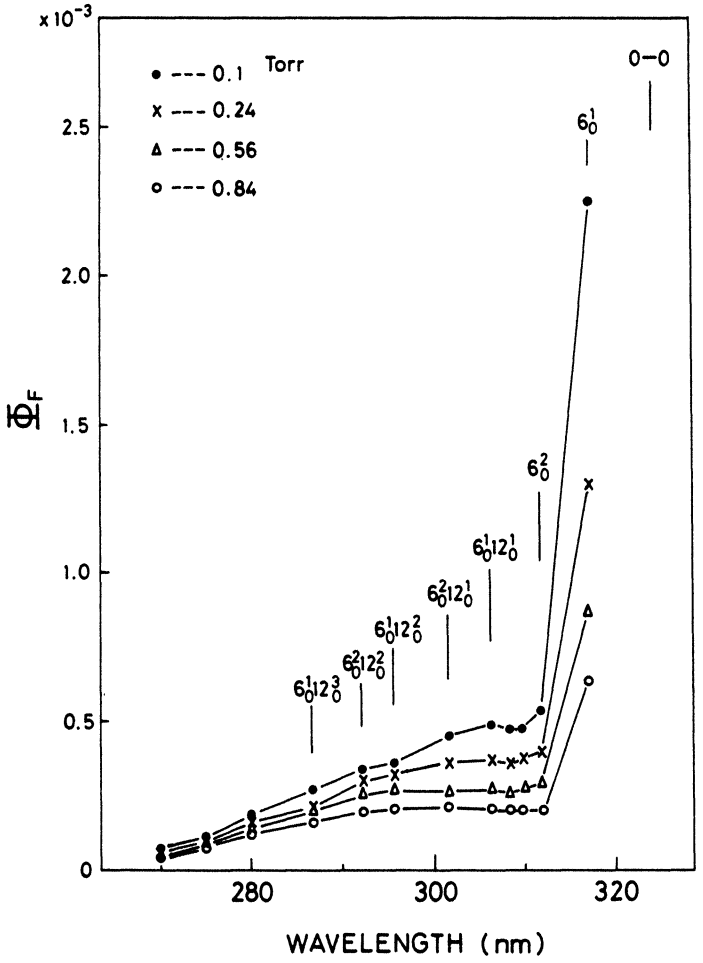

Figure 5 Excitation wavelength dependence of the fluorescence quantum yields of *s*-triazine vapor at different pressures: (•) 0.1 Torr; (×) 0.24 Torr; (Δ) 0.56 Torr; (O) 0.84 Torr.

The Stern-Volmer relation associated with the self-quenching of the fluorescence of *s*-triazine vapor is assumed to be expressed in the form

$$\frac{\Phi_{F_2}(0)}{\Phi_{F_2}(p)} = \frac{\Phi_F(0) - \Phi_{F_1}}{\Phi_F(p) - \Phi_{F_1}} = 1 + \langle k_c \rangle \langle \tau_{F_2}(0) \rangle p \tag{4}$$

where $\langle k_c \rangle$ is the average bimolecular rate constant for collisional quenching of the excited molecule and $\langle \tau_{F_2}(0) \rangle$ is the average lifetime of the slow component at $p = 0$. In Eq. (4), the average values of k_c and $\tau_{F_2}(0)$ are employed since the total emission which involves the IPL fluorescence and the broad fluorescence was monitored to

Table 1 Emission quantum yields, lifetimes and related quantities of *s*-triazine vapor.

Excitation wavelength (nm)	ΔE^a (cm^{-1})	Assignment	Φ_{F_1} (10^{-5})	$\Phi_{F_2}(0)$ (10^{-4})	Φ_p^b	τ_I (ps)	$\tau_{II}(0)$ (ns)	$\tau_{III}(0)$ (ns)	k^R ($10^5 s^{-1}$)	k_c^{II} (10^7 $s^{-1}Torr^{-1}$)	k_c^{III} (10^6 $s^{-1}Torr^{-1}$)	$\langle k_c \rangle \langle \tau_{F_2}(0) \rangle$ ($Torr^{-1}$)	k_{ISC} ($10^9 s^{-1}$)	k^{NR} ($10^9 s^{-1}$)
317	677	6^1	8.2	34	1.0	310	120	—	2.6	6.6	—	5.2	1.9	1.3
312	1,176	6^2	7.3	6.8	1.0	280	150	700	2.6	6.1	4.5	2.9	2.1	1.4
309.8	1,400		7.3	5.8	1.0	240	196	700	3.0	4.1	4.0	2.0	2.5	1.7
308.4	1,546		7.5	5.9	0.98	235	192	650	3.2	3.4	4.2	2.1	2.5	1.8
306.4	1,758	$6^1 12^1$	7.2	5.7	0.97	260	180	650	2.8	4.1	4.3	2.1	2.2	1.6
301.6	2,277	$6^2 12^1$	6.4	5.3	0.94	215	161	500	3.0	0.96	4.1	1.9	2.6	2.1
295.6	2,950	$6^1 12^2$	6.3	4.0	0.92	190	143	260	3.3	0.74	4.7	1.2	2.9	2.4
292.2	3,343	$6^2 12^2$	6.5	4.2	0.94	170	114	260	3.8	0.68	4.5	1.3	3.3	2.6
286.5	4,024	$6^1 12^3$	6.4	3.0	0.93	155	72	198	4.1	0.66	5.1	0.98	3.6	2.9
280	4,834		5.8	2.3	0.92	130	40[c]	100[c]	4.5	—	—	0.72	4.2	3.5
275	5,483		5.0	1.2	0.81	110	23[c]	85[c]	4.5	—	—	0.74	4.5	4.6
270	6,158		4.0	0.54	0.66	85	25[c]	65[c]	4.7	—	—	0.75	4.7	7.1
265	6,857		2.8	—	0.55	—	—	—	—	—	—	—	—	—
260	7,582		1.8	—	0.36	—	—	—	—	—	—	—	—	—

[a] The $S_0 \rightarrow S_1$ origin is at 30870 cm^{-1}.[13]
[b] The value for 317 nm excitation is normalized to unity.
[c] These values are the lifetimes obtained at 0.05 Torr.

obtain $\Phi_{F_2}(p)$. The reciprocal of the fluorescence intensity divided by a sample pressure, which corresponds to the reciprocal yield, is plotted in Figure 6 as a function of pressure. The Stern-Volmer plots for excitation into different vibronic levels are known to give straight lines. By the use both of the slope and of the intercept of these plots, $\langle k_c \rangle \langle \tau_{F_2}(0) \rangle$ and $\Phi_{F_2}(p)$ under collision-free conditions, $\Phi_{F_2}(0)$, were determined at representative excitation positions.

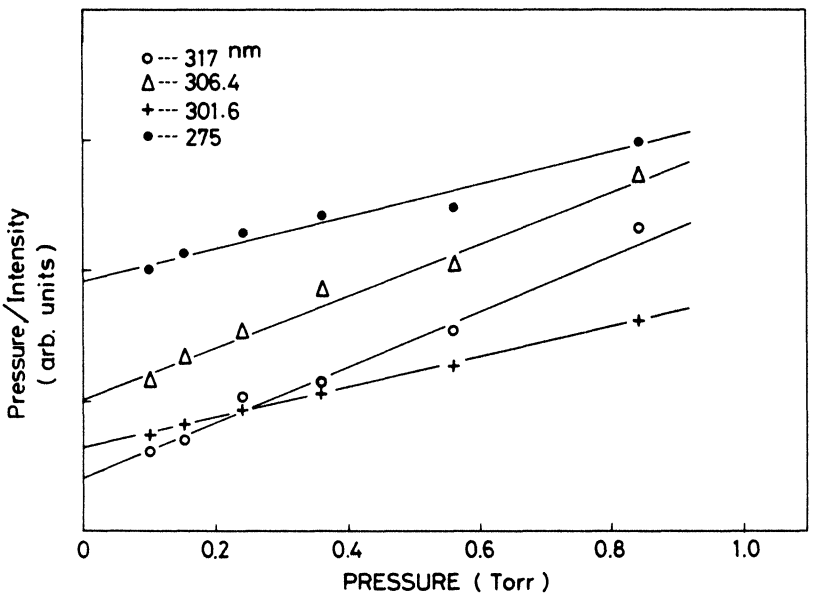

Figure 6 Plots of the reciprocal of the intensity of the slow fluorescence divided by the sample pressure against pressure for different excitation positions: (O) 317 nm: (Δ) 306.4 nm; (+) 301.6 nm; (•) 275 nm.

The excitation wavelength dependence of Φ_{F_1} and $\Phi_{F_2}(0)$ is shown in Figure 7. $\Phi_{F_2}(0)$ is known to decrease with increase of ΔE. It should be emphasized in particular that the 6_0^1 band at 317 nm exhibits a markedly high value of $\Phi_{F_2}(0)$. Φ_{F_1} slightly varies in the excitation-wavelength region above 280 nm, whereas Φ_{F_1} abruptly decreases with shortening excitation wavelength below 280 nm. Note that the present values of Φ_{F_1} were obtained with an excitation bandwidth of 0.3 nm and that the results are almost the same as with the previous ones obtained with an excitation bandwidth of 0.7 nm.[6]

The quantum yields both of the IPL fluorescence and of the fluorescence at 400 nm obtained across the rotational contour are shown in Figures 8 and 9 for the 6_0^1 and 6_0^2 bands, respectively. These spectra were obtained for a mixture of 0.2 Torr of *s*-triazine and 0.1 Torr of biacetyl. As reported in the previous paper,[1] $\Phi_{F_2}^{IPL}(p)$ varies greatly across the rotational contour (see Figures 8[*a*] and 9[*a*]). On the other

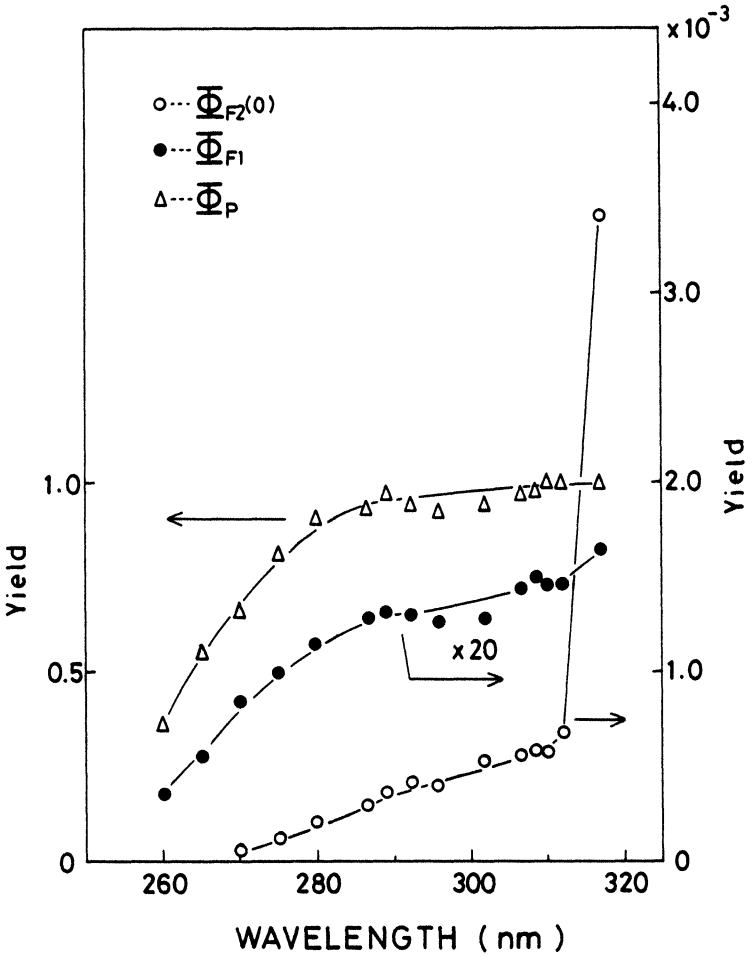

Figure 7 Excitation wavelength dependence of $\Phi_{F_2}(0)$ (O), Φ_{F_1} (●) and Φ_p (Δ). The values of Φ_{F_1} are multiplied by twenty, and Φ_p for 317 nm excitation is normalized to unity.

hand, $\Phi_{F_2}^{broad}$ is considered to be nearly independent of the rotational level excited, as suggested from less pronounced variation of the yield of the 400-nm emission (see Figures 8(*b*) and 9(*b*)). Figure 10 shows the quantum yield of the 400-nm emission across the rotational contour of the $6_0^1 12_0^1$ vibronic band at 306.4 nm. The yield is nearly constant across the rotational contour. The fluorescence following excitation into $6^1 12^1$ is dominated by the broad fluorescence, as is seen in Figure 3(*d*). Eventually, $\Phi_{F_2}^{broad}$ (*p*) is confirmed to be independent of the rotational level excited. At high pressures, the quantum yields of the IPL fluorescence and the fluorescence at 400 nm are almost flat across the rotational contour of these bands, indicating that both $\Phi_{F_1}^{broad}$ are independent of the rotational level excited.

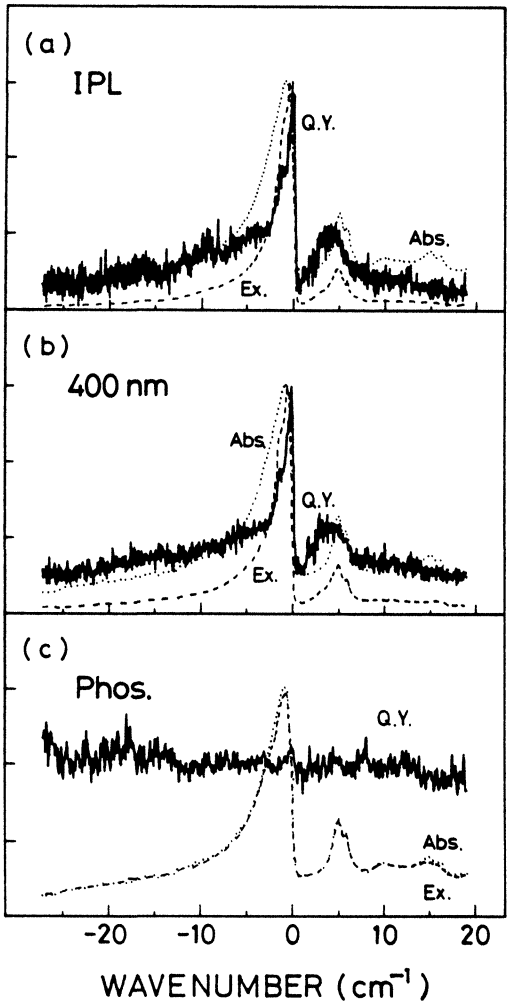

Figure 8 Spectra for the 6_0^1 band of *s*-triazine at 0.2 Torr in the presence of 0.1 Torr of biacetyl. (*a*) Excitation spectrum monitored through the IPL fluorescence at 340 nm (- - -) and the yield spectrum (—). (*b*) Excitation spectrum monitored through the fluorescence at 400 nm (- - -) and the yield spectrum (—). (*c*) Excitation spectrum monitored through the sensitized biacetyl phosphorescence at 510 nm (- - -) and the yield spectrum (—). In all cases, . . ., absorption spectrum at 5.7 Torr.

3.3. *Fluorescence Decays and Lifetimes*

Decays of the IPL fluorescence and the 400-nm emission are shown in Figures 11, 12 and 13 for excitation at the 6_0^1, 6_0^2 and $6_0^1 12_0^1$ bands, respectively. As reported in the previous paper,[1] the IPL fluorescence from 6^1 or 6^2 exhibits a biexponential decay composed of fast and slowly decaying portions (see Figures 11[*a*] and 12[*a*]). The same is true for the IPL fluorescence on excitation at the $6_0^1 12_0^1$ band, as is seen in

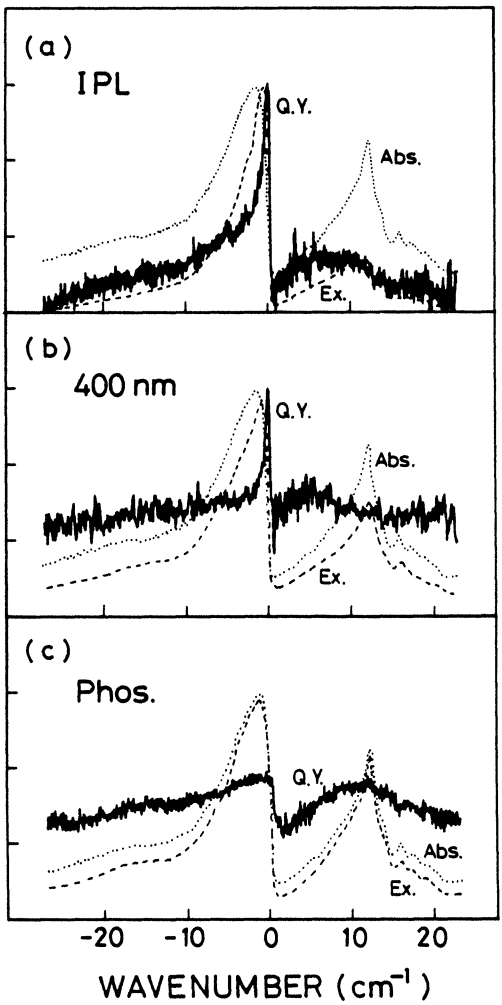

Figure 9 Spectra for the 6_0^2 band of s-triazine vapor obtained with the same sample as in Figure 8. (*a*) Excitation spectrum monitored through the IPL fluorescence at 330 nm (- - -) and the yield spectrum (—). (*b*) Excitation spectrum monitored through the fluorescence at 400 nm (- - -) and the yield spectrum (—). (*c*) Excitation spectrum monitored through the sensitized biacetyl phosphorescence (- - -) and the yield spectrum (—). In all cases, . . ., absorption spectrum at 5.7 Torr.

Figure 13(*a*). It is known from Figures 11(*b*), 12(*b*) and 13(*b*) that the broad fluorescence also involves fast and slow components which are analogous to the fast and slow components of the IPL fluorescence. In each of the IPL and broad fluorescence emissions, the fast and slow components will be denoted by component I and component II, respectively. The lifetime of the component I is very short, and will be described later. The lifetime values of the component II ($\tau_{II}[p]$) of the IPL fluorescence and the broad fluorescence are regarded as the same within the

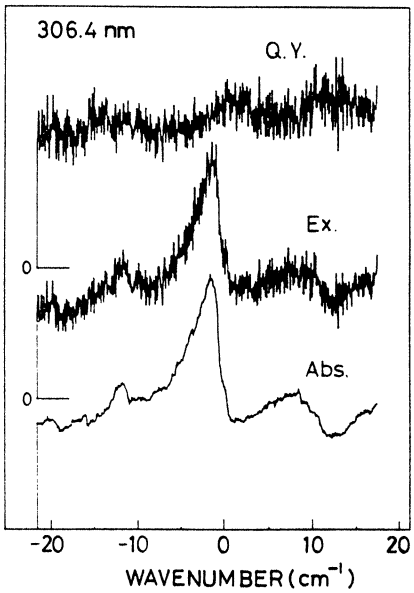

Figure 10 Absorption spectrum (bottom), fluorescence excitation spectrum (middle) and quantum yield spectrum (top) along the rotational contour of the $6_0^1 12_0^1$ band. Fluorescence was monitored at 400 nm for the sample of 0.1 Torr. Absorption spectrum is at 5.7 Torr.

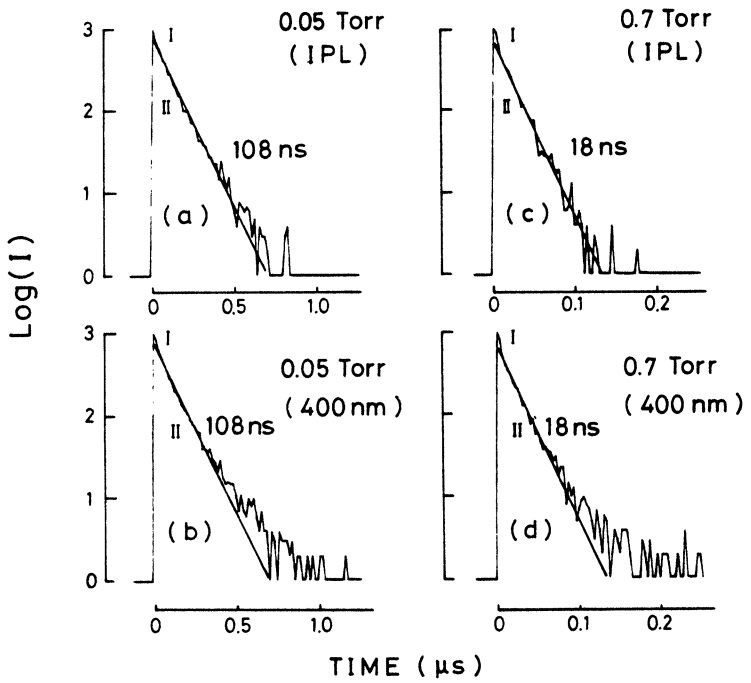

Figure 11 Fluorescence decays for *s*-triazine following excitation at the 6_0^1 band, obtained by monitoring the IPL fluorescence at 340 nm at 0.05 Torr (*a*) and 0.7 Torr (*c*) and obtained by monitoring the emission at 400 nm at 0.05 Torr (*b*) and 0.7 Torr (*d*). The lifetime values evaluated from the slope of the straight line are shown in the figure.

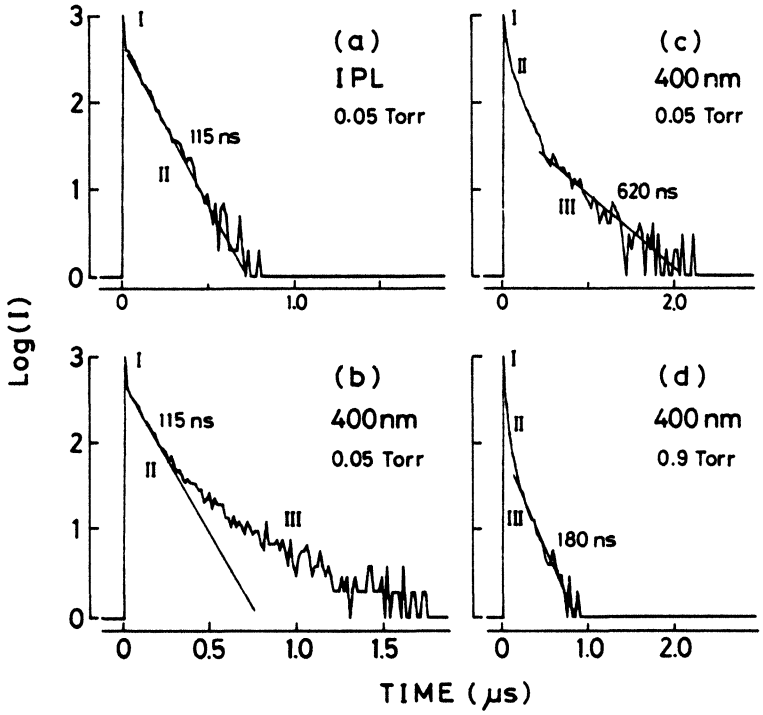

Figure 12 Fluorescence decays for *s*-triazine following excitation at the 6_0^2 band; (*a*) obtained by monitoring the IPL fluorescence at 330 nm at 0.05 Torr; (*b*) and (*c*) obtained by monitoring the emission at 400 nm at 0.05 Torr; (*d*) obtained by monitoring the emission at 400 nm at 0.9 Torr. Decays in (*a*) and (*b*) were obtained with a time resolution twice as high as in (*c*) and (*d*). The lifetime values evaluated from the slope of the straight line are shown in the figure.

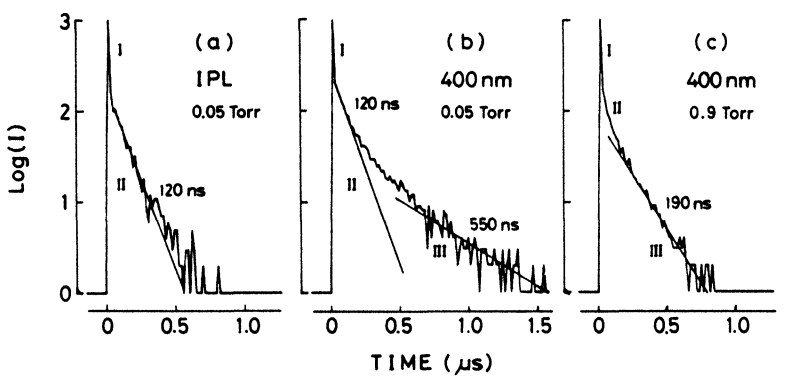

Figure 13 Fluorescence decays for *s*-triazine following excitation at the $6_0^1 12_0^1$ band: (*a*) obtained by monitoring the IPL fluorescence at 319.8 nm at 0.05 Torr; (*b*) and (*c*) obtained by monitoring the broad fluorescence at 400 nm at 0.05 Torr and 0.9 Torr, respectively. The lifetime values evaluated from the slope of the straight line are shown in the figure.

experimental error, and the values at 0.05 Torr are evaluated to be 108, 115 and 120 ns at 6^1, 6^2 and $6^1 12^1$, respectively. In contrast with the IPL fluorescence, the broad fluorescence involves another slow component, denoted by component III, whose lifetime ($\tau_{III}(p)$) is longer than that of component II at the same pressure. The pressure dependence of $\tau_{III}(p)$ is different from the one of $\tau_{II}(p)$. It should be noted that the component III is very weak on the 6_0^1 excitation, as is seen in Figures 11(*b*) and 11(*d*). On excitation at wavelengths below 300 nm, the IPL fluorescence could not be observed, but the shape of the decay of 400 nm emission is similar to the corresponding one on 306.4 nm excitation in the sense that components I–III exist at low pressures.

Plots of the reciprocal lifetimes of components II and III of the broad fluorescence against pressure are shown in Figure 14. Note that $\tau_{II}(p)$ of the IPL fluorescence is essentially the same as the one of component II of the broad fluorescence at the same excitation positions at the same p. In order to analyze the experimental results shown in Figure 14, we assume the following equations of the Stern-Volmer type:

$$1/\tau_{II}(p) = 1/\tau_{II}(0) + k_c^{II} p \tag{5}$$

$$1/\tau_{III}(p) = 1/\tau_{III}(0) + k_c^{III} p \tag{6}$$

where k_c^{II}, k_c^{III} are rate constants, for components II and III respectively, related to collision. On excitation at wavelengths above 300 nm, plots of $\tau_{II}(p)$ and $\tau_{III}(p)$

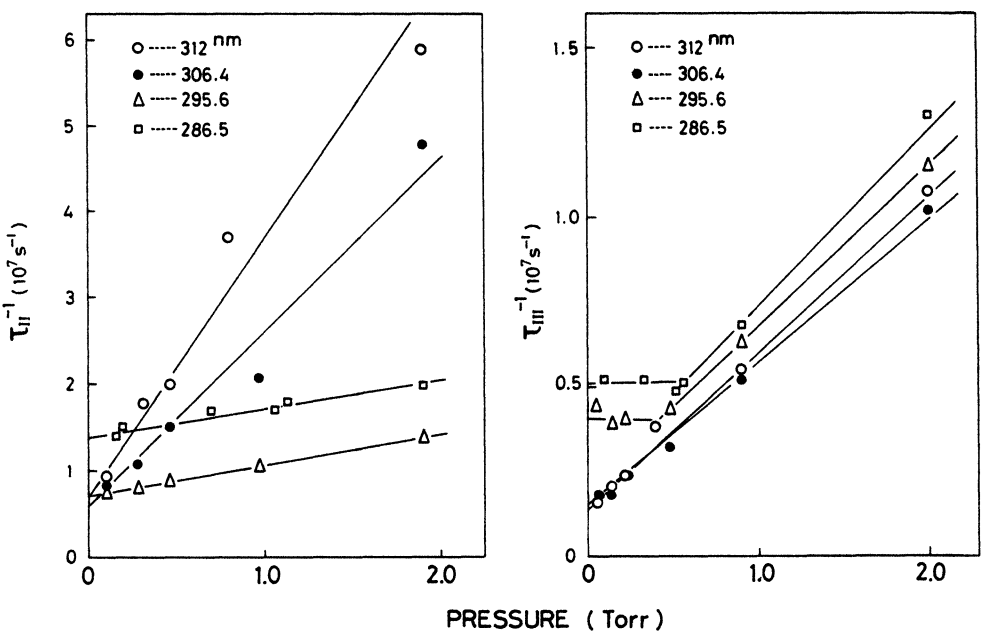

Figure 14 Plots of the reciprocal lifetimes of component II (left) and component III (right) of the broad fluorescence against pressure for different excitation wavelengths: (O) 312 nm; (•) 306.5 nm; (Δ) 295.6 nm; (□) 286.5 nm.

against p give a nearly straight line in the whole pressure region. Thus, Eqns (5) and (6) can be reasonably applied. At excitation wavelengths below 300 nm, plots of $\tau_{II}(p)$ vs. p also give a nearly straight line in the whole pressure region. Plots of $\tau_{III}(p)$ vs. p give a straight line at pressures above 0.5 Torr, but $\tau_{III}(p)$ is nearly independent of pressure below 0.5 Torr, as is seen in Figure 14. The values of k_c^{II} and k_c^{III} are shown in Figure 15 as a function of excitation wavelength, together with the values of $\langle k_c \rangle \langle \tau_{F_2}(0) \rangle$. The values of $\tau_{II}(p)$ and $\tau_{III}(p)$ under collision-free conditions, $\tau_{II}(0)$ and $\tau_{III}(0)$ respectively, are also shown in *Table 1*. As is seen in *Table 1*, k_c^{II} is larger than the hard sphere collision rate constant ($k_{hsc} \simeq 1 \times 10^7 s^{-1} \text{Torr}^{-1}$) by several times for excitation wavelengths above 300 nm, whereas k_c^{II} is nearly equal to k_{hsc} for excitation wavelengths below 300 nm. As is seen in Figure 15, k_c^{II} steeply decreases with increase of ΔE, but becomes flat at excitation wavelengths below 300

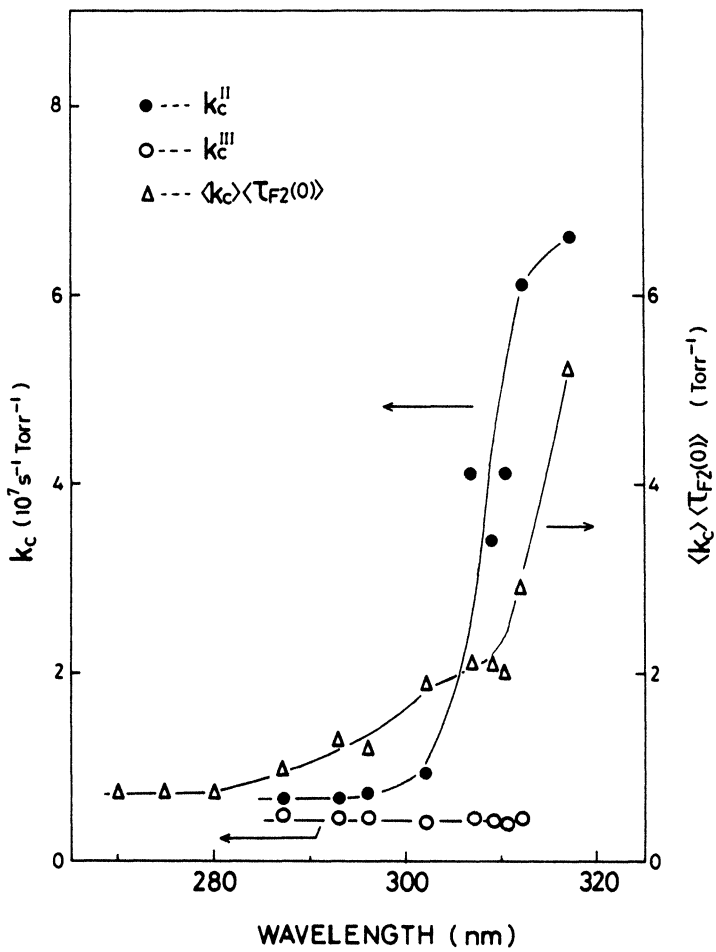

Figure 15 Plots of k_c^{II}, k_c^{III} and $\langle k_c \rangle \langle \tau_{F_2}(0) \rangle$ against excitation wavelength.

nm. It is also found that k_c^{III} is nearly equal to k_{hsc} for any excitation position. As is seen in Figure 15, $\langle k_c \rangle \langle \tau_{F_2}(0) \rangle$ shows an excitation wavelength dependence similar to that of k_c^{II}.

Emission decays of the fast component of *s*-triazine vapor were measured by monitoring the total emission with a sample of *s*-triazine (5.7 Torr) plus SF_6 (100 Torr). Figure 16 shows the curves of the fluorescence decay and the excitation pulse at two different excitation positions, together with the simulated curves. The

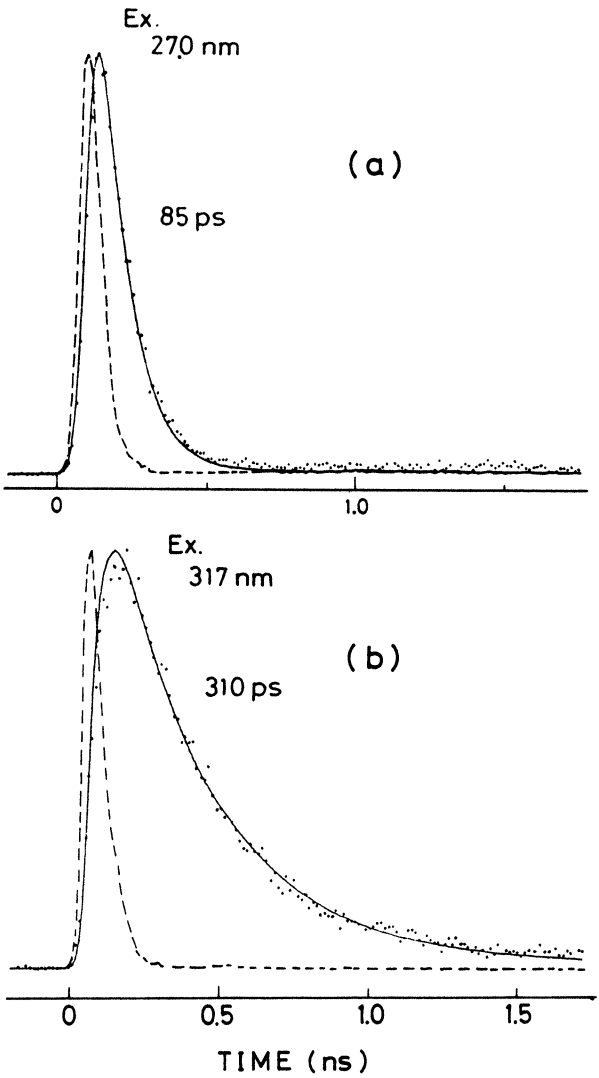

Figure 16 Dotted lines show the fluorescence decays for *s*-triazine vapor of 5.7 Torr in the presence of SF_6 of 100 Torr following excitation at 270 nm (*a*) and 317 nm (*b*). Simulated curves shown by the solid lines were obtained by convoluting the excitation pulse shape shown by the broken lines.

simulated curves were obtained by convoluting the profile of the excitation pulse with a single exponential decay constant and found to fit well the observed decay curves at every excitation position. It is emphasized that the slow fluorescence is almost completely quenched at ~100 Torr and that the observed decays correspond to component I. The evaluated lifetimes (τ_I) are shown in *Table 1*. It is seen from *Table 1* that τ_I decreases monotonically with increase of ΔE.

Fluorescence decay of *s*-triazine vapor in the bulk gas was also measured by Nott and Selinger[21] for excitation into four single vibronic levels of S_1. They reported a non-exponential decay, in agreement with the present work, but the presence of components I, II and III was not referred. The presence of the broad fluorescence besides the IPL fluorescence was not referred either. The measurements of the fluorescence lifetime in a free jet expansion were carried out by Heaven *et al.*[22] for excitation into selected vibronic levels of S_1. Their lifetimes ranging from 50 to 100 ns seem to correspond to $\tau_{II}(0)$ of the present experiments, though the total emission was monitored.

3.4. *Sensitized Biacetyl Phosphorescence Quantum Yield*

The excitation spectrum shown in Figure 4(*e*) was obtained by monitoring the sensitized biacetyl phosphorescence at 510 nm with a sample of mixtures of *s*-triazine (0.9 Torr), biacetyl (3 Torr) and SF_6 (100 Torr). The phosphorescence quantum yield, Φ_p, is plotted in Figure 7 as a function of excitation wavelength. These yields were obtained by comparing the excitation spectrum shown in Figure 4(*e*) with the absorption spectrum. Φ_p at high pressures is related to the triplet formation yield, as will be mentioned later. As is seen in Figure 7, Φ_p slightly decreases with increase of ΔE in the wavelength region above 280 nm. At wavelengths below 280 nm, however, Φ_p steeply decrease with increase of ΔE, indicating that a new channel of fast nonradiative process(es) other than intersystem crossing (ISC) opens at around 280 nm.

Rotational level dependence of Φ_p was also examined both at a low pressure of 0.3 Torr and at a high pressure of ~100 Torr. The results at low pressure are shown in Figures 8(*c*) and 9(*c*) for the 6_0^1 and 6_0^2 bands, respectively. These Φ_p spectra were obtained with the sample of mixture of *s*-triazine (0.2 Torr) and biacetyl (0.1 Torr). Note that the yield spectra of the IPL fluorescence shown in Figures 8(*a*) and 9(*a*) were obtained with the same sample as the spectra shown in Figures 8(*c*) and 9(*c*) were obtained. As is seen in Figures 8(*c*) and 9(*c*), Φ_p is nearly independent of the rotational level excited, in contrast with the yield of the IPL fluorescence. At ~100 Torr, Φ_p is also nearly flat along the rotational contour for every band.

4. DISCUSSION

The fluorescence of *s*-triazine vapor involves both the IPL fluorescence and the broad fluorescence. Each of the two types of fluorescence gives fast and slow components, I and II. The broad fluorescence gives another slow component, III, characterized by a less tendency to undergo collisional quenching. Thus, the present

results are very similar to the results for pyrimidine vapor obtained for excitation into S_1 vibronic levels with $\Delta E > 1000\ cm^{-1}$.[23] In pyrimidine, the emitting levels of the broad fluorescence have been assigned to S_1 vibronic levels which are isoenergetic to the IPL, that is, the broad fluorescence is attributed to the intramolecular vibrational redistribution within the S_1 manifold following excitation into the IPL.[23,24] As will be mentioned later, the assignment of the emitting levels of the broad fluorescence, U, in *s*-triazine vapor is different from the one in pyrimidine. However, the emission characteristics are very similar to each other. Then, the present results for *s*-triazine vapor seem to be interpreted with the kinetic scheme shown in Figure 17, which is essentially the same as employed for pyrimidine vapor.[23] Here, solid and wavy arrows represent radiative (R) and nonradiative (NR) processes, respectively. S represents the IPL. *Ta* stands for the triplet levels coupled directly to S, and *Tb* stands for the triplet levels other than *Ta that are quasidegenerate with* S and U. It is assumed that the number of *Ta* is much smaller than the total number of the triplet levels, $T(= Ta + Tb)$, isoenergetic to S and U, based on ro-vibronic selectivity on interaction between singlet and triplet levels.[20] With this scheme, quantum yields and time dependent intensities of fluorescence can be expressed in the three extreme cases.[23]

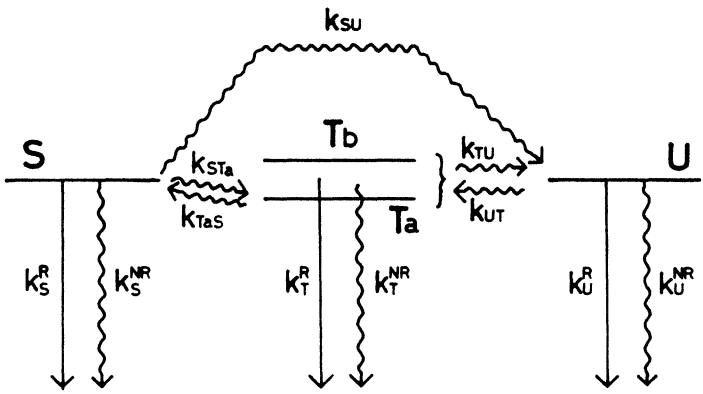

Figure 17 Kinetic schemes and various rate constants (k) for *s*-triazine. R and NR refer to radiative and nonradiative processes, respectively. See text for other symbols.

Case (1). This corresponds to the experiments under high pressure conditions. At high pressures, the collision-induced vibrational relaxation in the triplet state is to be very fast. Then, $T_a \rightarrow S$ and $T(T_a$ and $T_b) \rightarrow U$ are neglected in the scheme shown in Figure 17. As a result, only the fast component of fluorescent occurs. Under these conditions, time-dependent intensities of the IPL fluorescence (I_F^{IPL}) and the broad fluorescence (I_F^{broad}), fluorescence quantum yields of the fast component and triplet formation yield (Φ_T) are given as follows:

$$I_F^{IPL} \propto \exp(-k_S t) \tag{7}$$

$$I_F^{\text{broad}} \propto \{-\exp(-k_S t) + \exp(-k_U t)\} \tag{8}$$

$$\Phi_{F_1}^{\text{IPL}} = k_S^{\text{R}}/k_S \tag{9}$$

$$\Phi_{F_1}^{\text{broad}} = k_U^{\text{R}} k_{SU}/k_U k_S \tag{10}$$

$$\Phi_T = \frac{1}{k_s}\left(k_{STa} + \frac{k_{SU}k_{UT}}{k_U}\right) \tag{11}$$

where

$$\left.\begin{aligned} k_S &= k_S^{\text{R}} + k_S^{\text{NR}} + k_{STa} + k_{SU} \\ k_U &= k_U^{\text{R}} + k_U^{\text{NR}} + k_{\text{UT}} \end{aligned}\right\} \tag{12}$$

Case (2). This corresponds to the experiments at low pressures on excitation into S_1 levels with small ΔE. It is assumed that $k_S U$ is much smaller than k_{STa}, and the processes $U \rightarrow T$ are neglected. Then, decays and quantum yields of the fluorescence are given as follows:

$$I_F^{\text{IPL}} \propto \left\{\left(\frac{k_S - \lambda_2}{\lambda_1 - \lambda_2}\right) \exp(-\lambda_1 t) + \left(\frac{\lambda_1 - k_S}{\lambda_1 - \lambda_2}\right) \exp(-\lambda_2 t)\right\} \tag{13}$$

$$\begin{aligned} I_F^{\text{broad}} \propto \Bigg\{ & \frac{(k_S - \lambda_2)k_{SU} - k_{TaU}k_{STa}}{(\lambda_1 - \lambda_2)(k_U - \lambda_1)} \exp(-\lambda_1 t) \\ & + \frac{k_{SU}(k_{TA} - k_U) + k_{TaU}k_{STa}}{(k_U - \lambda_1)(k_U - \lambda_2)} \exp(-k_U t) \\ & + \frac{(\lambda_1 - k_S)k_{SU} + k_{TaU}k_{STa}}{(\lambda_1 - \lambda_2 (k_U - \lambda_2)} \exp(-\lambda_2 t) \Bigg\} \end{aligned} \tag{14}$$

$$\Phi_F^{\text{IPL}} = \frac{k_S^{\text{R}} k_{Ta}}{k_S k_{Ta} - K_{STa}k_{TaS}} \tag{15}$$

$$\Phi_F^{\text{broad}} = \frac{k_U^{\text{R}}(k_{TaU}k_{STa} + k_{SU}k_{Ta})}{k_U(k_S k_{Ta} - k_{TaS}k_{ST_a})} \tag{16}$$

$$\Phi_T = \frac{k_{STa}k_{Ta}}{k_S k_{Ta} - k_{STa}K_{TaS}} \tag{17}$$

where

$$\left.\begin{aligned} \lambda_{1,2} &= \tfrac{1}{2}\left\{(k_S+k_{Ta}) \pm \sqrt{(k_S-k_{Ta})^2+4k_{TaS}k_{STa}}\right\} \\ k_S &= k_S^{\mathrm{R}} + k_S^{\mathrm{NR}} + k_{STa} + k_{SU} \\ k_U &= k_U^{\mathrm{R}} + k_U^{\mathrm{NR}} \\ k_{Ta} &= k_{Ta}^{\mathrm{R}} + k_{Ta}^{\mathrm{NR}} = k_{TaS} = k_{TaU} \end{aligned}\right\} \tag{18}$$

Here, k_{TaU}, $k_{\mathrm{Ta}}^{\mathrm{R}}$ and k_{Ta}^{NR}, which are not explicitly expressed in the scheme shown in Figure 17, are the rate constant of reverse ISC from *Ta* to *U*, radiative and nonradiative rate constants in *Ta*, respectively.

Case (3). This corresponds to the experiments at low pressures on excitation into S_1 levels with large ΔE. It is assumed that $k_{STa} \ll k_{SU}$, and the interaction between S and *Ta* is neglected. Then, the fluorescence is considered to be dominated by the broad fluorescence.

According to the kinetic scheme, yield and decay of the broad fluorescence are given by

$$\mathrm{I}_F^{\mathrm{broad}} \propto \left\{ (k_T - k_S) \exp(-k_t) + \frac{(k_T-\gamma_1)(\gamma-(k_S)}{(\gamma_1-\gamma_2)} \exp(-\gamma_1 t) + \frac{(k_T-\gamma_2)(k_S-\gamma_1)}{(\gamma_1-\gamma_2)} \exp(-\gamma_2 t) \right\} \tag{19}$$

$$\Phi_F^{\mathrm{broad}} = \frac{k_U^{\mathrm{R}} k_{SU} k_T}{k_S(k_U k_T - k_{TU}k_{UT})} \tag{20}$$

where

$$\left.\begin{aligned} \gamma_{1,2} &= \tfrac{1}{2}\left\{ (k_U + k_T) \pm \sqrt{(k_U - k_T)^2 + 4k_{UT}k_{TU}} \right\} \\ k_S &= k_S^{\mathrm{R}} + k_S^{\mathrm{NR}} + k_{SU} \\ k_T &= k_T^{\mathrm{R}} + k_T^{\mathrm{NR}} + k_{TU} \\ k_U &= k_U^{\mathrm{R}} + k_U^{\mathrm{NR}} + k_{UT} \end{aligned}\right\} \tag{21}$$

Interpretation of the Emission Properties

According to Eq. (7), the fast component of the IPL fluorescent exhibits an exponential decay due to $\exp(-k_S t)$. Equation (8) indicates that the fast component of the broad fluorescence also shows an exponential decay due to $\exp(+k_U t)$, preceded by a rise due to $-\exp(-k_S t)$. In fact, an exponential decay is observed for the fast component of fluorescence at any excitation position, as is seen in Figure 16.

As will be mentioned later, the rate of IVR is very fast. As a result, the rise of the fast fluorescence could not be observed even when the emission is dominated by the broad fluorescence.

In the present study, the total emission was monitored to obtain the decay profile of the fast fluorescence. Φ_{F_1} was also obtained by monitoring the total emission. Accordingly, an apparent radiative decay constant, k^R, may be defined by the use of Φ_{F_1} and τ_I.

$$k^R = \Phi_{F_1}/\tau_I \tag{22}$$

The values of k^R at the different excitation wavelengths are shown in *Table 1*. When the IPL fluorescence is dominant, Φ_{F_1} corresponds to $\Phi_{F_1}^{IPL}$ and k^R is approximately equal to k_S^R. When the broad fluorescence is dominant, Φ_{F_1} corresponds to $\Phi_{F_1}^{broad}$, and k_R is considered to be nearly equal to k_U^R. When the intensities of the IPL fluorescence and the broad fluorescence are close to each other, the simple treatment based on Eq. (22) is no longer proper, but the k^R values evaluated with Eq. (22) may be considered to lie between k_S^R and k_U^R. Thus, k^R is reasonably regarded as the average radiative rate constant at the emitting levels of the total fluorescence.[6]

In Case (2), the IPL fluorescence gives fast and slow components, I and II, with lifetimes $1/\lambda_1$ and $1/\lambda_2$, respectively, as is seen in Eq. (13). By assuming that $\lambda_1 > k_U > \lambda_2$ in Eq. (14), the broad fluorescence is known to give a biexponential decay preceded by a rise. k_U and λ_2 in Eq. (14) give the reciprocal lifetimes of components I and II of the broad fluorescence, respectively. Thus, the lifetime of the component II of the broad fluorescence is regarded as the same as the component II of the IPL fluorescence.

The fluorescence properties at low pressure on excitation into 6^1 seem to correspond to Case (2). Both the IPL fluorescence and the broad fluorescence exhibit a biexponential decay with components I and II. The lifetimes of the component II are the same for both emissions, in agreement with Eqs. (13) and (14).

In Case (3), the broad fluorescence is characterized by a rise due to $-\exp(-k_s t)$, a fast decay due to $\exp(-\gamma_1 t)$ and a slow decay due to $\exp(-\gamma_2 t)$, as is seen in Eq. (19). Note that $\gamma_1 > \gamma_2$. On excitation at wavelengths below 300 nm, only the broad fluorescence is observed. Further, the broad fluorescence exhibits both the fast and slow components, as expected in Case (3). In contrast with the results derived from Eq. (19), however, the slowly decaying portion of the broad fluorescence involves components II and III whose self-quenching rates are different from each other.

In the present treatment of Case (3), it is assumed that all the levels of *U* to which IVR occurs from the IPL are coupled to the triplet levels in the same manner. Actually, each of the *U* levels may be coupled to the triplet levels in each manner even when *U* is prepared under the collision-free conditions. For example, some *U* levels may be coupled to *Ta*, and the *U* levels remaining may be coupled to other triplet levels, i.e., *Tb*. In such a case, two slow components whose lifetimes are different from each other would appear. Thus, the presence of the multicomponents in the slowly decaying portion of the broad fluorescence suggests that *U* levels are coupled to the triplet levels in the different manners from each other.

For excitation at the bands at 312, 309.8, 308.4 and 306.4 nm, both the IPL

fluorescence and the broad fluorescence are observed, and the former emission exhibits a biexponential decay composed of components I and II, in agreement with Eq. (13). The broad fluorescence exhibits component II whose lifetime is essentially the same as component II of the IPL fluorescence besides the fast component I, in agreement with Eq. (14). Further, the broad fluorescence involves the slow component III. The component II of the broad fluorescence for these excitations is reasonably attributed to the reverse ISC from *Ta* to *U*, whereas the component III may be attributed to the reverse ISC to *U* from the triplet levels other than *Ta*, i.e., *Tb*. Thus, the fluorescence properties at low pressures on these excitations can be classified as the intermediate between Case (21) and Case (3). In fact, S_1 levels reached by these excitations have moderate ΔE.

According to the quantum mechanical treatment, the reciprocal lifetime of the slow component of the IPL fluorescence under collision-free conditions is roughly given by[1,3,4,20]

$$\tau_{II}(0)^{-1} \simeq (\Gamma_T + \Gamma_S/N)/\hbar \tag{23}$$

where Γ_T and Γ_S represent at zero pressure the total energy widths of the triplet state and S respectively, and N gives the number of the triplet levels coupled to S. Similarly, the reciprocal lifetime of the slow component of the broad fluorescence may be given by Eq. (23) with Γ_U/M instead of Γ_S/N. Here, Γ_U and M represent the total energy width of U and the number of the triplet levels coupled to U, respectively. The value of $\tau_{II}(0)$ is much smaller than the value of $\tau_{III}(0)$ on each excitation, as is seen in *Table 1*. Accordingly, component II is attributed to the *S–Ta–U* mixed levels, whereas component III is attributed to the *U–Tb* mixed levels. It should be again emphasized that the number of *Tb* is much larger than that of *Ta*. In the extreme case that N (or M) $\rightarrow \infty$, the lifetime of the slow fluorescence is equal to the lifetime of the pure triplet state, as is known in Eq. (23). Accordingly, $\tau_{III}(0)$ is considered to be very close to the lifetime of the pure triplet state which is isoenergetic to the IPL under collision-free conditions.

The maximum value of Φ_T at high pressure was reported by Knight and Parmenter[25] to be 0.6. By employing the Φ_p values shown in *Table 1*, therefore, values of Φ_T at high pressure are given by

$$\Phi_T = 0.6\Phi_p \tag{24}$$

Note that the maximum of Φ_p, obtained for 317 nm excitation, is normalized to unity in *Table 1*. When $k_{STa} \gg k_{SU}$ in Case (1), the rate constant of ISC which occurs from the IPL, k_{ISC} ($= k_{STa}$), is given, based on Eqs. (7) and (11), by

$$k_{ISC} = \Phi_T/\tau_I \tag{25}$$

When $k_{SU} \gg k_{STa}$ in Case (1), the rate constant of ISC following IVR, k_{ISC} ($= k_{UT}$), is also given by Eq. (25), based on Eqs. (8) and (11). Even when k_{STa} is close to k_{SU}, the rate constant of ISC from the singlet state to the triplet state is also given by Eq. (25) by assuming that $k_{STa} \simeq k_{UT}$ and that $k_U + {}_{SU} \simeq k_S$ in Eq. (11). According to Eq. (25), k_{ISC} values were evaluated for various excitation positions. The results are shown in *Table 1*.

According to Eqs. (7), (8) and (12), the difference between the reciprocal lifetime of the fast component and k_{ISC} obtained just above gives the rate constant, denoted by k_R^N, of nonradiative process(es) other than ISC or IVR which occurs from the singlet state. When $k_{STa} \gg k_{SU}$, k^{NR} corresponds to k_S^{NR}, whereas k^{NR} corresponds to k_U^{NR} when $k_{SU} \gg k_{STa}$. The values of k^{NR} evaluated on each excitation are also shown in *Table 1*.

Vibrational Level Dependence of Intramolecular Dynamics

Let's first discuss the excited vibronic level dependence of IVR. The intensity ratio of the IPL fluorescence to the broad fluorescence abruptly increases with increase of ΔE, as is seen in *Figure 3*. At high pressures, this ratio gives k_U/k_SU by assuming that $k_S^R \simeq k_U^R$, as is seen in Eqs. (9) and (10). Further, k_U is considered to be very close to $1/\tau_I$ at any excitation position. For excitation into 6^1, the IPL fluorescence is dominant, and τ_I was determined to be 310 ps (see *Table 1*). Therefore, the rate constant of IVR, K_{SU}, at 6^1 is regarded as much smaller than $3.2 \times 10^9\ s^{-1}$. For excitation into 6^2, the IPL fluorescence is comparable in intensity to the broad fluorescence, and τ_I was determined to be 280 ps. As a result, k_{SU} at 6^2 is roughly estimated to be $3.6 \times 10^9 s^{-1}$. On excitation at 309.8 or 306.4 nm, the intensity of the IPL fluorescence is roughly estimated to be several % of the intensity of the broad fluorescence, and τ_I was determined to be about 250 ps (see *Table 1*). Then k_{SU} for these excitations is considered to be $\sim 1 \times 10^{11}\ s^{-1}$. For excitation at wavelengths below 300 nm, the IPL fluorescence is not observed. Then, k_{SU} is considered to be larger than $10^{12} s^{-1}$ for these excitations. Thus, present results indicate that the IVR rate abruptly increases with increase of ΔE. Pallix and Colson[26] reported that IVR occurs in $\ll 5$ ps for 306.4 nm excitation, based on the time-resolved photoelectron studies, in fair agreement with our present results.

As seen in *Table 1*, k^R increases monotonically with increase of ΔE. As reported in the previous paper,[6] therefore, it is conceivable that the emitting levels of the broad fluorescence, *U*, are not vibronic levels belonging solely to S_1, but are mixed levels which are composed not only of vibrational levels belonging to S_1 but also of the ones belonging to another electronic state, probably $^1A_2''(n\pi^*)$ state.

As is seen in *Table 1*, the rate constant of ISC, k_{ISC}, monotonically increases with increasing ΔE in the whole excitation wavelength region. It is also seen in *Table 1* that the rate constant of nonradiative process(es) other than ISC or IVR from the singlet state, k^{NR}, gradually increases with increase of ΔE in the region above 280 nm and that k^{NR} steeply increases with increase of ΔE in the region below 280 nm. The latter process(es) may be assigned to the internal conversion from the excited singlet state to the ground state and/or photochemical processes. The sudden increase of k^{NR} at around 280 nm implies that a new channel for the nonradiative process(es) opens at S_1 levels with ΔE of $\sim 5000\ cm^{-1}$.

As mentioned previously, the value of $\tau_{III}(0)$ is considered to be very close to the lifetimes of the triplet state near the IPL under collision-free conditions. Accordingly, a monotonic decrease of $\tau_{III}(0)$ with increase of ΔE suggests that the lifetime of the triplet state monotonically decreases with increase of ΔE.

$\Phi_{F_2}(0)$ monotonically decreases with increase of ΔE, except for excitation into 6^1, as is seen in Figure 4. According to the quantum mechanical treatment, $\Phi_{F_2}^{IPL}(0)$ is related to N, i.e., the larger N becomes, the smaller $\Phi_{F_2}^{IPL}(0)$ becomes. Similarly, $\Phi_{F_2}^{broad}(0)$ may be related to M. Accordingly, present results indicate that the effective number of the triplet levels coupled to the singlet level increases monotonically with increase of ΔE. These conclusions are well understood by considering the monotonic increase of the triplet level density with increase of ΔE. However, $\Phi_{F2}(0)$ at 6^1 is extraordinarily large in comparison with other values of $\Phi_{F2}(0)$, indicating that the effective number of the triplet levels suddenly increase on going from 6^1 to 6^2. As suggested from the presence of component III of the slow fluorescence on excitation into 6^2 and other higher vibronic levels, M is regarded as much larger than N. Therefore, the sudden decrease of $\Phi_{F_2}(0)$ on going from 6^1 to 6^2 is related to the IVR since the intensity of the broad fluorescence is comparable to or larger than the intensity of the IPL fluorescence for excitation into 6^2 and other higher vibronic levels. Recall that the total emission which involves both the IPL fluorescence and the broad fluorescence was monitored to obtain $\Phi_{F_2}(0)$.

Rotational Level Dependence of Intramolecular Dynamics

At first, excited rotational level dependence of each of the rate constants shown in Figure 17 is discussed, based on the rotational level dependence of the emission quantum yields. Hereafter, excited rotational level is denoted by ERL. $\Phi_{F_1}^{IPL}$ is nearly independent of ERL, and the radiative rate constant is considered to be independent of ERL. Based on Eq. (9), therefore, k_S is known to be independent of ERL. When $k_{STa} \gg k_{SU}$ in Case (1), k_{STa} is given by $\Phi_T k_S$ according to Eq. (11). Then, the results that Φ_p at high pressure is flat across the rotational contour of the 6_0^1 band indicate that k_{STa} is independent of ERL. Note that Φ_T at high pressure is given by Eq. (24). When $k_{STa} \ll k_{SU}$, K_S of Eq. (12) is nearly equal to $k_{STa} + k_S^{NR}$. Then, k_S^{NR} is known to be independent of ERL since k_S *and* k_{STa} are independent of ERL. When $k_{SU} \ll k_{STa}$, $\Phi_{F_1}^{broad}$ and Φ_T are given by k_U^R/k_U and k_{UT}/k_U, respectively, according to Eqs. (10) and (11). Accordingly, the results that both $\Phi_{F_1}^{broad}$ and Φ_P at high pressure are flat across the rotational contour of the $6_0^1 12_0^1$ band suggest that k_U, k_{UT} and k_U^{NR} are independent of ERL. Note that k_U^{NR} is approximately given by $k_U - k_{UT}$. k_S of Eq. (12) is approximately given by $k_{SU} + k_S^{NR} + k_{STa}$, and k_{SU} at 6^2 is regarded as close to $k_S^{NR} + k_{STa}$, as mentioned previously. Further, k_U, k_S^{NR} and k_{STa} are independent of ERL. Then, the results that $\Phi_{F_1}^{broad}$ is nearly flat across the rotational contour of the 6_0^2 band, combined with Eq. (10), suggest that k_{SU} is independent of ERL.

$\Phi_{F_2}^{IPL}$, i.e., Φ_F^{IPL} at low pressure, varies greatly along the rotational contour. Accordingly, k_{TaS} is known to depend remarkably on ERL, based on Eq. (15). In contrast with Φ_F^{IPL}, Φ_F^{broad} is nearly independent of ERL at any pressure. Accordingly, k_{TU} is known to be independent of ERL, based on a comparison between Eqs. (15) and (20). As far as only k_{TaS} depends on ERL, a variation both of Φ_F^{broad} of Eq. (16) and of Φ_T of Eq. (17) was shown in the previous paper[23] to be small compared with that of Φ_F^{IPL} of Eq. (15). In fact, Φ_F^{broad} and Φ_T at low pressure are nearly flat

across the rotational contour both for the 6_0^1 and for the 6_0^2 bands. Thus, ERL dependence of the emission quantum yields indicates in the kinetic scheme shown in Figure 17 that k_{TaS} markedly depends on ERL and that other rate constants are independent of ERL.

It is mentioned about the collision-induced rotational relaxation (CIRR) within S_1 since CIRR may wipe out the rotational level dependence of the emission quantum yield. When an inert gas, e.g., SF_6 is employed as a collision partner, the rate constant of CIRR is considered to be nearly equal to k_{hsc}, though the rate constant of CIRR in S_1 may be larger than k_{hsc} for ground-state s-triazine as a collision partner. In the present experiments, SF_6 was used for pressurizing the sample vapor. Then, the product of the rate constant of CIRR and the pressure of SF_6 is given by 1×10^9 s^{-1} at 100 Torr which is the maximum pressure employed, by assuming that the rate constant of CIRR is 1×10^7 s^{-1} $Torr^{-1}$ for SF_6 as a collision partner. Thus, the CIRR rate is much slower than the dephasing decay rate in S_1 even at 100 Torr. Note that τ_1 is shorter than ~300 ps at any excited level, as is seen in *Table 1*. Accordingly, CIRR within S_1 is considered to be not so important in the present experiments.

According to the quantum mechanical treatment, a remarkable variation of $\Phi_{F_2}^{IPL}$ along the rotational contour comes from ERL dependence of N. In the previous paper,[1] it was suggested that N is proportional to $2J + 1$ since K scrambling occurs in ISC from the IPL to the triplet state (J and K are the rotational quantum numbers of the total angular momentum excluding the nuclear spin and its projection on the top axis, respectively).

When N is proportional to $2J + 1$, it will be reasonable to consider that the number of the triplet levels coupled to each of U levels is also proportional to $2J + 1$. Then, question arises: Why does $\Phi_{F_2}^{broad}$ show less ERL dependence in contrast with $\Phi_{F_2}^{IPL}$?, i.e., why is k_{TU} independent of ERL in contrast with k_{TaS}? According to our polarization measurements, the broad fluorescence is nearly depolarized for any excitation along the rotational contour of the 6_0^1 and 6_0^2 bands, suggesting that K scrambling occurs for IVR of *s*-triazine vapor.[16] Through IVR from the IPL specified by rotational quantum numbers (J', K'), therefore, not only U levels with J' and K' but also U levels with J' and K other than K' are regarded as simultaneously prepared. Then, each of U is considered to be coupled to the triplet levels whose number is proportional to $2J' + 1$. Similarly, each of the triplet levels coupled to a U level specified by $<J', K')$ is considered to be coupled also to other U levels with J' and K other than K' which are prepared through IVR. Then, the number of the triplet levels coupled to U, M, relative to the total number of U prepared through IVR are regarded as independent of ERL when K scrambling occurs in IVR. Eventually, the fact that $\Phi_{F_2}^{broad}$ is independent of ERL suggests that K scrambling occurs not only in ISC but also in IVR, in agreement with the fluorescence polarization measurements.[16]

Quenching Mechanism of Slow Fluorescence

Let's first discuss the mechanism of the quenching of fluorescence in intermediate case molecules. According to the kinetic model, the slow fluorescence components,

II and III, are described by reversible conversion between the singlet and triplet levels, as is seen in Figure 17. In terms of a quantum mechanical treatment of the behavior of the intermediate case molecules, the components II and III are emitted from mixed levels composed of singlet and triplet levels, as mentioned previously. Obviously, collisional transfer from the singlet-triplet mixed levels to other pure triplet levels results in fluorescence quenching. Even when collisional transfer occurs from the singlet-triplet mixed levels to other mixed levels, fluorescence quenching may occur when the singlet character of the initial mixed level is larger than the other.

For excitation at wavelengths above 300 nm, both IPL fluorescence and broad fluorescence are observed, and component II of the IPL fluorescence is quenched by a collision in the same manner as the component II of the broad fluorescence. However, there is a substantial difference in rate of collisional quenching between components II and III of the broad fluorescence. The values of k_c^{II} are several times as large as k_{hsc}, whereas k_c^{III} is nearly equal to k_{hsc}. As mentioned previously, component II of the IPL fluorescence and the component II of the broad fluorescence are regarded as emitted from the mixed levels composed of *S, U* and *Ta*. The number of *Ta* is smaller than the total number of the triplet levels isoenergetic to *S* and *U*. Hence a weak collision will be enough to transfer *s*-triazine molecules from the *S–Ta–U* mixed levels either to pure triplet levels or to other mixed levels with less singlet character, resulting in the fluorescence quenching. Then, the quenching of component II of the broad fluorescence, as well as component II of the IPL fluorescence, for excitation at wavelengths above 300 nm is related to the collision-induced rotational relaxation.

At higher vibronic levels, the singlet ro-vibronic level density is so high that a hard collision will be required to transfer the molecules from the single-triplet mixed levels to pure triplet levels since any triplet levels may couple to some of the singlet levels at these higher levels. This accounts for the observation that slow components, II and III, have a collisional quenching constant as small as k_{hsc}, for excitation at wavelengths below 300 nm. Then, the fluorescence quenching for these excitations is related to the collision-induced vibrational relaxation.

Actually, the broad fluorescence exhibits components II and III on excitation at wavelengths below 300 nm whose quenching rate constants are different from each other. These two components are regarded as emitted from the mixed levels composed of *U* and a part of the triplet state and from the mixed levels composed of U and all the triplet levels isoenergetic to *U*, respectively. Collisional transfer from the former mixed level to the latter may induce a fluorescence quenching since the singlet character in the former may be larger than the other. However, such a collisional transfer does not lead to an effective quenching since the collisional transfer from *U–T* mixed levels to other *U–T* mixed levels is followed by the fluorescence. The results that k_c^{II} and k_c^{III} at excitation wavelengths below 300 nm are as small as k_{hsc} and that k_c^{II} is a lttle larger than k_c^{III} are understood by considering such circumstances.

On excitation at wavelengths above 300 nm, component III of the broad fluorescence whose k_c^{III} is as small as k_{hsc} exists besides the component II whose k_c^{II} is much

larger than k_{hsc}. These results suggest that a part of U levels are coupled to all of the triplet levels isoenergetic to the IPL even for these excitations, as mentioned previously.

5. CONCLUSION

In addition to the IPL fluorescence, broad fluorescence is observed on excitation into 6^1 and other higher vibronic levels of S_1. Both emissions exhibit a decay composed of fast and slowly decaying portions which is characteristic of the intermediate case molecules. The intensity of the broad fluorescence relative to the IPL fluorescence abruptly increases with increase of ΔE, indicating that the IVR rate abruptly increases with increase of ΔE. The broad fluorescence is regarded as emitted from the mixed levels composed of S_1 vibronic levels and vibronic levels belonging to other electronic state following IVR from the IPL. The lifetime of the triplet state, the ISC rate, the rate of the nonradiative process(es) other than ISC or IVR from the singlet state and the emission quantum yields markedly depend on the vibrational level excited. $\Phi_{F_2}^{IPL}$ markedly depends on the rotational level excited, whereas other emission quantum yields are independent of the rotational level excited, indicating that K scrambling occurs both in ISC and in IVR. At lower vibronic levels of S_1, a collision-induced rotational relaxation plays an important role for the fluorescence quenching, whereas a collision-induced vibrational relaxation plays an important role for the quenching of fluorescence following excitation into higher vibronic levels of S_1.

Acknowledgment

The author thanks emeritus Professor H. Baba for his interest and continuous encouragement. The author thanks Professors K. Yoshihara and I. Yamazaki and Dr. T. Murao for their help in measuring fluorescence lifetime in the picosecond region. This work was partly supported by the Ministry of Education, Science and Culture, for Grant-in-Aid for Scientific Research on Priority Areas.

References

1. N. Ohta and H. Baba, *Chem. Phys.* **82**, 41 (1983).
2. H. Saigusa and E. C. Lim, *J. Chem. Phys.* **78**, 91 (1983).
3. F. Lahmani, A. Tramer and C. Tric, *J. Chem. Phys.* **60**, 4431 (1974).
4. R. van der Werf and J. Kommandeur, *Chem. Phys.* **16**, 125 (1976).
5. N. Ohta and H. Baba, *Chem. Phys. Lett.* **106**, 382 (1984).
6. N. Ohta and H. Baba, *Chem. Phys. Lett.* **112**, 212 (1984).
7. K. Chihara and H. Baba, *Bull. Chem. Soc. Japan* **48**, 3093 (1975).
8. H. Baba, M. Fujita, N. Ohta and Y. Shindo, *J. Spectrosc. Soc. Japan* **29**, 387 (1980).
9. N. Ohta and H. Baba, *J. Chem. Phys.* **76**, 1654 (1982).
10. W. H. Melhuish, *J. Phys. Chem.* **65**, 229 (1961).
11. E. Lippert, W. Nagele, I. Seibold-Blankenstein, U. Staiger and W. Voss, *Z. Anal. Chem.* **170**, 1 (1959).
12. T. Murao, I. Yamazaki and K. Yoshihara, *Appl. Opt.* **21**, 2297 (1982).
13. G. Fischer and G. J. Small, *J. Chem. Phys.* **56**, 5934 (1972).
14. J. Barnard, Ph.D. Thesis, University College, London (1974), and references therein.
15. J. D. Webb, K. M. Swift and E. R. Bernstein, *J. Chem. Phys.* **73**, 4891 (1980).

16. N. Ohta, O. Sekiguchi and H. Baba, *J. Chem. Phys.* **88**, 68 (1988).
17. N. Ohta, M. Fujita, T. Takemura, Y. Shindo and H. Baba, *Chem. Phys. Lett.* **97**, 81 (1983).
18. A. Frad, F. Lahmani, A. Tramer and C. Tric, *J. Chem. Phys.* **60**, 4419 (1974).
19. K. Uchida, I. Yamazaki and H. Baba, *Chem. Phys. Lett.* **38**, 133 (1976).
20. K. G. Spears and M. El-Manguch, *Chem. Phys.* **24**, 65 (1977).
21. P. R. Nott and B. K. Selinger, *Aust. J. Chem.* **31**, 1889 (1978).
22. M. Heaven, T. Sears, V. E. Bondybey and T. A. Miller, *J. Chem. Phys.* **75**, 5271 (1981).
23. O. Sekiguchi, N. Ohta and H. Baba, *Bull. Chem. Soc. Japan* **59**, 3405 (1986).
24. B. E. Forch, K. T. Chen, H. Saigusa and E. C. Lim, *J. Phys. Chem.* **87**, 2280 (1983).
25. A. E. W. Knight and C. S. Parmenter, *Chem. Phys.* **15**, 85 (1976).
26. J. B. Pallix and S. D. Colson, *Chem. Phys. Lett.* **119**, 38 (1985).